Cerebral Cortex, July 2018;28: 2563–2576

doi: 10.1093/cercor/bhy081
Advance Access Publication Date: 21 April 2018
Original Article

ORIGINAL ARTICLE

Neural Coding of Cell Assemblies via Spike-Timing Self-Information

Meng Li[1], Kun Xie[1,2], Hui Kuang[1], Jun Liu[1], Deheng Wang[1,2], Grace E. Fox[1], Zhifeng Shi[3], Liang Chen[3], Fang Zhao[1,2], Ying Mao[3] and Joe Z. Tsien[1,2]

[1]Brain and Behavior Discovery Institute and Department of Neurology, Medical College of Georgia at Augusta University, Augusta, GA 30912, USA, [2]The Brain Decoding Center, Banna Biomedical Research Institute, Yunnan Province Academy of Science and Technology, Xi-Shuang-Ban-Na Prefecture, Yunnan 666100, China and [3]Department of Neuropathology, Huashan Hospital, Fudan University, Shanghai 200040, China

Address correspondence to Meng Li, Email: limeng.braindecoder@gmail.com; Joe Z. Tsien, Email: jtsien@augusta.edu

Abstract

Cracking brain's neural code is of general interest. In contrast to the traditional view that enormous spike variability in resting states and stimulus-triggered responses reflects noise, here, we examine the "Neural Self-Information Theory" that the interspike-interval (ISI), or the silence-duration between 2 adjoining spikes, carries self-information that is inversely proportional to its variability-probability. Specifically, higher-probability ISIs convey minimal information because they reflect the ground state, whereas lower-probability ISIs carry more information, in the form of "positive" or "negative surprisals," signifying the excitatory or inhibitory shifts from the ground state, respectively. These surprisals serve as the quanta of information to construct temporally coordinated cell-assembly ternary codes representing real-time cognitions. Accordingly, we devised a general decoding method and unbiasedly uncovered 15 cell assemblies underlying different sleep cycles, fear-memory experiences, spatial navigation, and 5-choice serial-reaction time (5CSRT) visual-discrimination behaviors. We further revealed that robust cell-assembly codes were generated by ISI surprisals constituted of ~20% of the skewed ISI gamma-distribution tails, conforming to the "Pareto Principle" that specifies, for many events—including communication—roughly 80% of the output or consequences come from 20% of the input or causes. These results demonstrate that real-time neural coding arises from the temporal assembly of neural-clique members via silence variability-based self-information codes.

Key words: cell assembly, interspike-interval, neural codes, neural self-information, spike timing

Introduction

A central theme in brain research is to understand how perception, memories and actions are dynamically represented in real time by the firing patterns of neurons. However, neurons in the brain discharge action potentials, or spikes, with enormous variability in both resting states and across trials in response to identical stimuli (Adrian and Zotterman 1926; Shadlen and Newsome 1994; Stein et al. 2005; Lin et al. 2006b; Faisal et al. 2008; Rolls and Deco 2010). Such a variability has been widely regarded as noise, because it undermines reliable real-time decoding of stimulus identities using the current "rate-code" or synchrony-based "temporal-code" methods (Lee et al. 1998; Stein et al. 2005; Averbeck et al. 2006; Faisal et al. 2008; Rolls and Deco 2010; Hartmann et al. 2015; Kanitscheider et al. 2015; Kohn et al. 2016). Yet, neurons in slice preparations are known to be capable of generating precisely-timed spikes in response

to currents injections at the soma (Mainen and Sejnowski 1995; Abbott and Sejnowski 1999). Thus, firing variability is not due to imprecision in spike generation at the soma per se. Moreover, studies in the primary visual or motor cortex showed that noise variability exhibited a certain level of correlation, perhaps reflecting attentional states or intent (Arieli et al. 1996; Abbott and Dayan 1999; Petersen et al. 2003; Wehr and Zador 2003; Churchland et al. 2010; Luczak et al. 2013; Marcos et al. 2013; Lin et al. 2015; Scholvinck et al. 2015; Saberi-Moghadam et al. 2016). Despite a renewed interest in neuronal variability, researchers typically treated firing variability as noise and removed it by applying over-trial data-averaging methods, for example, peritime stimulus histogram (PTSH) as a way to assess tuning properties of the recorded units. Such an averaging procedure inherently ignores any information possibly encoded in the temporal structure of the spike train. The time-zero used in PTSH analysis, marking the stimulus onset by outside observers, simply does not reflect the intrinsic operation of neurons sitting inside the brain. Therefore, one would naturally wonder, what is the neural code capable of being intrinsic to neurons themselves? How does such a neural code work in the face of enormous real-time firing variability?

We recently proposed the Neural Self-Information Theory that the brain uses interspike-interval (ISI) variability as the self-information messenger to generate real-time neural code at the cell-assembly level (Li and Tsien 2017). In essence, the ISI, or the silence duration between 2 adjoining spikes, carries self-information that solely depends on its inverted relation to its probability against the neuron's ISI variability history. Under this self-information principle, higher-probability ISIs reflect the ground state and convey less information, whereas lower-probability ISIs carry more information, in the form of positive or negative surprisals, signifying the excitatory or inhibitory shifts away from the ground state, respectively. Together with the ground state, these surprisals constitute the information quanta, enabling ternary construction of real-time neural code (Li and Tsien 2017). Real-time cognitions and behaviors are the expressions of temporally coordinated surprisals emitted by cell assemblies which are organized by a power-of-two-based permutation logic (Li et al. 2016; Tsien 2015; Xie et al. 2016).

Here, we applied this self-information concept and developed a general and unbiased decoding strategy to uncover cell-assembly patterns in the prelimbic cortex, anterior cingulate cortex (ACC), and hippocampal CA1 of freely-behaving mice. These cell assemblies spanned from those encoding "categorical variables" such as earthquake, foot-shock, elevator drop, or 5-choice visual-discrimination behaviors, as well as encoding "continuous variables," such as spatial navigation or sleep cycles. Our analyses further revealed the conserved critical boundaries from which lower-probability ISIs emerge as self-information packets to generate robust, real-time, cell-assembly neural code.

Materials and Methods

Ethics Statement

All animal work described in the study was carried out in accordance with the guidelines laid down by the National Institutes of Health and was approved by the Institutional Animal Care and Use Committee of Augusta University (Approval AUP number: BR07-11-001) and Banna Biomedical Research Institute (BBRI-15 001).

In Vivo Recording in Mice and Data Processing

The 128-channel tetrodes and headstages were used to record from the basolateral amygdala (BLA), dorsal striatum, CA1, ACC, retrosplenial cortex (RSC) and prelimbic cortex (PRL), bilaterally, with 64 channels per hemisphere in freely-behaving mice as previously described (Lin et al. 2006a; Xie et al. 2016). For facilitating the identification of the electrode array position, the electrode tips were dipped in fluorescent Neuro-Dil (Neuro-DiI, #60 016, red oily solid color, from Biotium, Inc.) which can then reveal the electrode track. Neuronal activities were recorded by the MAP system (multichannel acquisition processor system, Plexon Inc., Dallas, TX). Extracellular action potentials and local field potentials (LFP) data were recorded simultaneously and digitized at 40 and 1 kHz, respectively. The artifact waveforms were removed, and the spike waveform minima were aligned using the Offline Sorter 2.0 software (Plexon Inc., Dallas, TX), which resulted in more tightly clustered waveforms in a principal component space. Spike sortings were done with the MClust 3.3 program with an auto-clustering method (KlustaKwik 1.5). Only units with clear boundaries and less than 0.5% of the spike intervals within a 1 ms refractory period were selected. The stability of the in vivo recordings was judged by waveforms at the beginning, during and after the experiments. Well-separated neurons were assessed by "Isolation Distance" and "L-ratio" (Schmitzer-Torbert et al. 2005). Neurons whose "Isolation Distance" > 15 and "L-ratio" < 0.7 were selected for the present analyses.

ISI-Based Cell-Assembly Decoding Method

The ISI-based Cell-Assembly Decoding (iCAD) involves 3 distinct steps (also see Supplementary Material): The first step was to use a gamma-distribution model to describe the variability of the neuron's ISI (Maimon and Assad 2009); the second step was to use the independent-component analysis (ICA) method to decode the ensemble patterns from the population-surprisal code by searching joint-variability surprisals; and the third step was to identify corresponding cell assemblies by examining top large-weight neurons, which can be directly identified by their weights in the demixing matrix $\mathbf{W}$ of the ICA analysis. Neurons' contribution in the corresponding cell assemblies was calculated as their normalized weights (in a range of 0–1) according to their weights in the demixing matrix.

Fearful Events and Corresponding Data Analysis

Mice were subjected to 3 fearful episodic events—earthquake, footshock, and free-fall drop (see Supplementary Material for a detailed description). These episodic stimuli are fearful as evidenced by physiological indications, including a rapid increase in heart rate, as well as a reduced heart-rate variability (Liu et al. 2013, 2014). To maintain the consistency of stimulation timing (minimizing the possible prediction of upcoming stimuli), the stimuli were triggered by a computer and delivered at randomized intervals within 1–3 min. After the completion of all fearful event sessions, the mouse was placed back into the home cage.

Sleep and Corresponding Data Analysis

Data were recorded when the mouse was sleeping in the home cage. The recorded LFP were first processed by the FPAlign (a utility program provided by Plexon Inc.) to correct the filter-induced phase delays. LFP channels recorded in the CA1 pyramidal cell layer were selected by judging the maximum yield of ripple during the animal's slow-wave sleep (SWS) and comparing the coherence in the theta-frequency and gamma-frequency band (Buzsaki et al. 2003). Further analyses were carried out with these LFP data offline by custom-written MATLAB (MathWorks) programs. The LFP was band-passed at Delta (2–4 Hz), Theta (4–10 Hz),

low Gamma (25–90 Hz), fast Gamma (90–130 Hz), and hippocampal ripples (130–200 Hz) by the Hamming window-based FIR filters with the order of 30 (see Supplementary Material for a detailed description).

Linear Track and Corresponding Data Analysis

A linear track experiment used a 100 cm × 1 cm closed runway. The exploration duration was 20 min. Real-time positions of the mouse were automatically tracked by CinePlex Behavioral Research Systems (Plexon Inc., Dallas, TX). Place fields were defined as a set of ≥5 contiguous pixels with a firing rate above 2 standard deviations of the mean firing rate. All spatial firing plots were smoothed with a 5 × 1 Gaussian smoothing filter using the MATLAB software (see Supplementary Material for a detailed description).

Five-Choice, Visual-Discrimination, Operant-Conditioning Task and Corresponding Data Analysis

The animal was introduced to a custom-designed test chamber equipped with 5 response apertures that can illuminate and a food magazine to deliver the reward. A trial was initiated by the mouse entering the food magazine. A brief light-stimulus was then presented in 1 of 5 possible apertures after a 5-s inter-trial interval (ITI) had elapsed. The mouse was required to scan the 5 apertures for the appearance of the light-stimulus and to respond in the "correct" aperture with a nose-poke response in order to earn a single food pellet delivered in the food magazine. If the mouse responded before the stimulus ("premature response") or in an adjacent, incorrect aperture ("incorrect response"), a 5-s time-out (TO) period was introduced by extinguishing the house light and not providing a food reward. Failure to respond within the limited hold (LH) period resulted in an "omission" and a subsequent 5-s TO period. After collecting the reward or—on punished trials—at the end of the TO period, a head entry in the food magazine would start a new trial. The mouse was pre-trained to achieve ≥ 50 correct trials within 30 min with > 80% accuracy and < 20% omissions before recording from the prefrontal cortex began. The animal's movements were recorded by CinePlex Behavioral Research Systems (Plexon Inc., Dallas, TX), and the animal's locations and head directions were tracked manually afterward. A detailed protocol was described in Supplementary Material.

Results

Neuronal Variability is Large During Cognition, But Diminished Upon Anesthesia

We measured neuronal variability from ISIs distribution using 3 well-defined statistics, namely, the coefficient of variation (CV), skewness, and kurtosis (see Materials and Methods). In probability theory and statistics, CV is a standardized measure of dispersion of a probability distribution, and skewness is a measure of the asymmetry of a probability distribution, whereas kurtosis is a measure of the "tailedness" of a probability distribution. For comparison purposes, "normal distribution" (indicating stochastic process) has CV = mean/std, Skewness = 0, and Kurtosis = 0, while "exponential distribution" (indicating Poisson process) has CV = 1, Skewness = 2, and Kurtosis = 6. The more skewed/long-tailed a distribution exhibits, the larger the CV, skewness and kurtosis it has.

If neuronal variability reflects "system noise," one would predict that variability in the principal-projection neurons should grow larger as information is transmitted from low subcortical structures to high-cognition cortices. On the other hand, if neuronal variability acts as the self-information generator, as the Neural Self-Information Theory posits, it should remain similar across various brain regions during cognitions, but should be diminished upon general anesthesia (Li and Tsien 2017).

Our measurement of spike variability of putative principal-projection cells (Fig. S1) in the BLA, hippocampal CA1, dorsal striatum (STR), RSC, PRL, and ACC found that principal-projection cells in these 6 different mouse brain regions exhibited similar neuronal variability distributions (Figs S2*A*,*B* and S3*A*-*D*). Furthermore, we recorded activity patterns of large numbers of cells from the BLA and CA1, respectively, in the awake state, as well as under ketamine/domitor-induced anesthesia. We found that putative pyramidal cells in both regions drastically decreased their neuronal variability upon anesthesia (Figs S2*C*,*D* and S3*E*,*G*).

ISI-Based Cell-Assembly Decoding Strategy to Uncover Cell Assemblies

The Neural Self-Information Theory posits that any given ISI inherently carries a discrete amount of information based on its ISI (the silence time duration) in an inverted relationship with the ISI variability-probability distribution. In other words, higher-probability ISIs convey less information because they reflect the ground state, whereas lower-probability ISIs carry more information, in the form of positive surprisals or negative surprisals, signifying the excitatory or inhibitory shifts from the ground state, respectively. The amount of self-information ("SI") contained in each ISI can be quantitatively obtained based on the ISI variability-distribution probability (SI = −log[*P*], where *P* is the probability) (Li and Tsien 2017). Under this self-information framework, real-time neural coding of cognitions and behaviors are the intrinsic states when temporally coordinated ISI surprisals emerge across cell-assembly members. Accordingly, we devised a general decoding strategy—termed ISI-based Cell-Assembly Decoding (iCAD) method—consisting of the following 3 major steps (Fig. 1):

- *To convert ISI variations into real-time variability surprisals*:
  Because ISI variability in many neural circuits conforms to the gamma distribution (Maimon and Assad 2009; Li et al. 2018), we first fitted a single neuron's ISIs with a gamma-distribution model, which can assign each neuron's ISI with a probability. Subsequently, a spike train emitted by a neuron can be transformed into a surprisal-based ternary code (positive surprisal as 1, ground state as 0, negative surprisal as −1) to describe the dynamic evolution in self-information states (Fig. 1*A*).
- *To uncover joint ISI surprisal patterns in space and time*:
  This step searches for joint-variability surprisals in both space (across simultaneously recorded cells) and time (moment-to-moment dynamics). Blind source separation (BSS) methods, such as the ICA, can be used to efficiently identify a set of independent information sources from simultaneously observed signals as structured patterns or relationships. Although the nature of the demixing matrix's dimension *p* meant that *p* information sources can be theoretically decoded from population activity, we reasoned that optimal neural coding should also be energy efficient via utilizing the least amount of variability surprisals together with the minimal number of such information-coding cells. As such, we used the minimal CV values in each dataset to unbiasedly assess the optimal

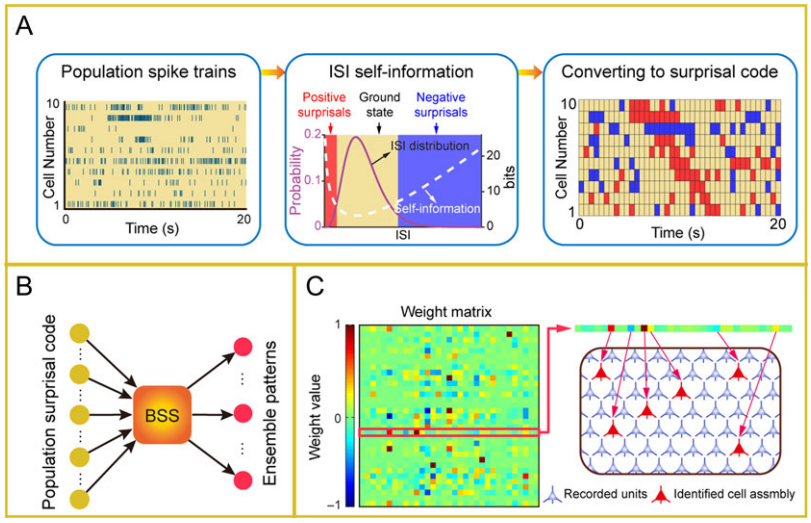

Figure 1. Self-information neural code-based decoding approach to uncover cell assemblies in the brain. (*A*) Step 1: Converting ISIs into real-time variability surprisals. The spike activities of 10 simultaneously recorded cells are illustrated in the left subpanel, the ISIs of each cell are fitted by the gamma-distribution model which assigns each ISI with a probability. Based on the fitted gamma-distribution model, 2 boundaries are then used (as shown in the middle subplot) to generate 3 states (ternary code); that is, positive-surprisal state (short silence, 1), negative-surprisal state (long silence, −1), and the balanced excitation–inhibition state (the ground state, 0). As such, neurons' spike trains can be converted into ternary surprisal codes (positive surprisal as 1 [red blocks], ground state as 0 [yellow blocks] and negative surprisal as −1 [blue blocks]). (*B*) Step 2: Uncovering joint surprisal patterns among simultaneously recorded units. Taking population ternary surprisal code as input, the ensemble patterns were unbiasedly discovered by the blind source separation (BSS) method which aims for searching joint variability-surprisals in both space (across simultaneously recorded cells) and time (moment-to-moment dynamics). (*C*) Step 3: Identifying corresponding cell assemblies by searching for the match with behaviors, external stimulation/events, internal states (LFP), etc. For each decoded independent signal source, neurons' information contributions are scaled quantitatively by the absolute values in the weight matrix W of BSS analysis (shown in the left subpanel), thus the resulting cell assemblies can be identified by picking up top-weight cells (right subpanel).

numbers of independent information sources (distinct cell assemblies) (Fig. 1*B*; also see Fig. S4*A*, Materials and Methods).

- *To identify corresponding cell assemblies*: This step will search how each independent signal source decoded by BSS may match a distinct real-time activation pattern given by a cell assembly using various parameters, such as LFP, the time points of stimulus presentations, or video tapes of an animal's behavioral state, specific actions and performance, or spatial locations, etc. The top-ranking memberships with the highest contribution weights in the cell assembly can be directly identified from the demixing matrix **W** (Fig. 1*C*; also see Fig. S4*B*). Moreover, their contributions to a given cell-assembly pattern can be quantitatively defined by shuffling techniques (i.e., by shuffling or artificially changing spike patterns to alter surprisal states). This step allowed us to assess quantitative membership information that other dimensionality-reduction-based pattern-classification methods (i.e., principal-component analysis or multiple-discriminant analysis) could not provide.

Identification of Cortical Cell Assemblies Encoding Fear-Memory Experiences

Neural coding (representation) of external and internal states are typically divided into 2 major categories—namely, continuous variables (i.e., arm movement, spatial navigation, sleep) and categorical variables (i.e., distinct stimuli or episodic events). To examine the usefulness of the iCAD method, we set out to uncover various cell assemblies related to both categories from multiple brain circuits.

First, we asked whether we could use the iCAD method to identify real-time coding of discrete categorical variables, such as distinct fearful experiences. We employed 128-channel tetrodes to monitor the spike activity of large numbers of the ACC, a subregion of the prefrontal cortex known to process emotions and fear memories (Steenland et al. 2012; Xie et al. 2013; Bliss et al. 2016), while subjecting the recorded mice to earthquake, footshock, and a sudden elevator drop—which are known to produce fear memories and fearful physiological responses (Liu et al. 2014). By scanning through the real-time spike dataset that contained 146 well-isolated, simultaneously recorded ACC units, our iCAD method automatically uncovered 3 distinct ensemble patterns (Fig. 2*A*). Specifically, ACC assembly-1 activations were time-locked to the occurrences of 6 earthquake events; ACC assembly-2 was temporally corresponding to 6 footshock events; and ACC assembly-3 was matched to free-fall events. Their unique ensemble patterns were further verified by shuffling their top 20% large-weight neurons' firing patterns with the Gaussian signal using the same mean firing rate and standard deviation (Fig. S5*A*). This shuffling procedure showed that the ensemble representation of a given event (e.g., free-fall) gradually became weaker as more top-contributing neurons were shuffled, while leaving the other 2 ensemble patterns (e.g., representing the earthquake and footshock) unchanged. Perievent spike raster and histogram plot analyses (Fig. S5*B*) revealed that while the majority of member cells exhibited event-specific responses (i.e., earthquake-specific, free-fall-specific, or footshock-specific ACC cells), some of the top cell-assembly members participated in 2 cell assemblies or even all 3 assemblies (Fig. 2*B*–*E*). Moreover, we examined the stability of cell-assembly memberships, and we calculated the weight matrix using the first 3 trials and compared them with the weight matrix obtained from the fourth to the sixth trial. We found that the vast majority of cell-assembly members remained stable (~75%) (Fig. S6). Correlation analysis further demonstrated that the weights of cell-assembly members between the first and second halves were highly correlated (the

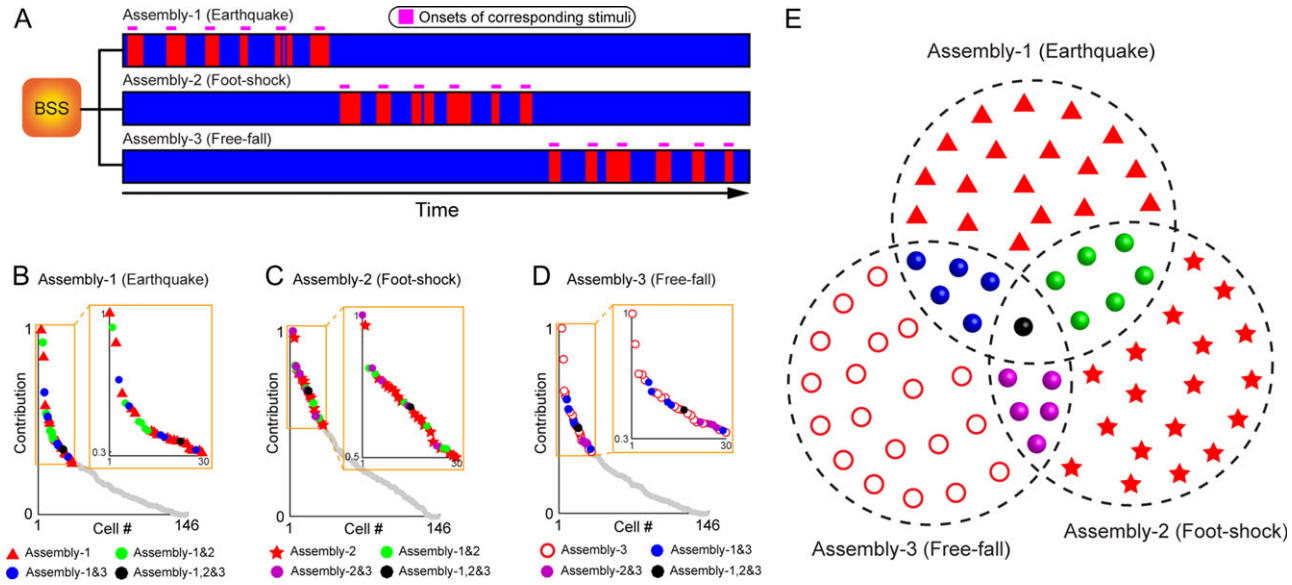

Figure 2. ACC cell assemblies encoding earthquake, footshock, or free-fall experiences. (*A*) Three cell assemblies were decoded from the mouse ACC representing earthquake, footshock or free fall experiences. Each cell assembly corresponded to the occurrences of 1 of 3 fearful events (6 trials per event, indicated by 6 purple bars above each ensemble pattern). (*B*) Cell membership analyses of Assembly-1 show that some neurons participated one specific assembly or multiple cell-assemblies (colored circles). Neurons' contribution in the corresponding cell assemblies was calculated as their normalized weights (in a range of 0–1) according to their weights in the demixing matrix. The top 30 units are shown in the zoomed-in box. Nonmember cells are marked in gray. 146 well-isolated and stable units were simultaneously recorded. (*C*) Assembly-2 corresponded to footshock. (*D*) Assembly-3 corresponded to free-fall. (*E*) Overlapping and nonoverlapping memberships among 3 cell assemblies underling earthquake, footshock, and free fall experiences.

correlation coefficient was about 0.8 for all 3 cell assemblies). These observations suggest that the top-weighted cell-assembly members remained largely stable in all 3 cases.

Identification of Cell Assemblies Related to Sleep Oscillations

Next, we investigated whether the self-information coding concept could be used to identify cell-assembly patterns related to internally driven, continuous variable processes such as sleep. Sleep is often defined by changes in EEG or LFP oscillations (Cantero et al. 2003). Thus, we asked whether the iCAD method could be used to identify cell assemblies in the CA1 related to various cycles of sleep. We scanned a 20-min spike dataset collected from the mouse hippocampal CA1 region during a sleep session and analyzed the ISI variability of 266 units recorded simultaneously using 128-channel tetrode arrays. Our iCAD method unveiled a total of 3 major ensemble patterns over the course of a 20-min sleep period (Fig. 3A). To search for the relationships of these 3 assembly patterns and sleep oscillations, we aligned these CA1 temporal patterns with the time-course plot of the simultaneously recorded LFP oscillations. Interestingly, we found that the temporal emergence of Cell Assembly-1 patterns was tightly matched to the occurrences of theta oscillation (Fig. 3B), whereas Cell Assembly-2 patterns were time-locked to ripple oscillation (Fig. 3C). Furthermore, we found that the activation of Cell Assembly-3 temporally corresponded to the DOWN-state of sleep cycles (Fig. 3D), that is, this ensemble pattern was consistently time-locked with the troughs of various LFP frequency bands.

Interestingly, we found that the top 20% ranking units (with largest weights in the demixing matrix $\mathbf{W}$) in CA1 Assembly-1 cells consisted of mostly putative interneurons (Fig. 3E, $n = 53$ cells). The shuffling technique (replacing their firing pattern with a Gaussian signal with the same mean firing rate and standard deviation) revealed that the Assembly-1 pattern was abolished as these top 20% contribution cells' firing patterns were shuffled (Fig. S7A). We noted that only about 15% of these Assembly-1 cells (8 cells, identified as putative O-LM cells or basket cells/bistratified cells based on the multiple criteria for interneuron subclassification, see Fig. S7B and S7C) exhibited a robust phase-locking relationship with theta oscillations (termed as Theta-coupled Assembly-1 cells) (Fig. S7B and S7C), which is consistent with evidence from literature that CA1 interneurons exhibited theta-coupling (Csicsvari et al. 1999; Somogyi and Klausberger 2005; Klausberger and Somogyi 2008; Kuang et al. 2010; Colgin 2016). Surprisingly, many Assembly-1 cells (45 cells, ~85% in Assembly-1) were not phase-locked with theta phase, rather they exhibited a significant difference in averaged firing rates between theta epochs versus nontheta epochs. One major group of the rate-altering cells, classified as putative Bursty cells (17 cells) (Fig. S7D), dramatically increased their firings during theta cycles in comparison to nontheta epoch, whereas 2 putative pyramidal cells significantly decreased their firings during theta sleep cycles (Fig. S7E).

Another surprising finding was that many theta-coupled CA1 cells from the simultaneously recorded dataset did not belong to Assembly-1. These nonmember theta cells were intriguingly distinct from those Assembly-1 theta cells as confirmed by their significant differences in firing correlation (Fig. S8A). This suggests that theta-coupling does not necessarily indicate the common membership. In fact, 2 distinct populations of theta interneurons exist in the CA1, with one subset uniquely engaged in sleep theta. Similarly, we noted that there were many rate-altering cells that did not belong to Assembly-1. Their distinct memberships were further supported by a dramatic statistical difference in the correlation coefficient between rate-altering member cells and rate-altering nonmember cells (Fig. S8B).

We then analyzed the nature of CA1 Assembly-2 ensemble patterns which were tightly time-locked with ripple peaks (Fig. 3C). In contrast to Assembly-1, the majority of the top Assembly-2 cells

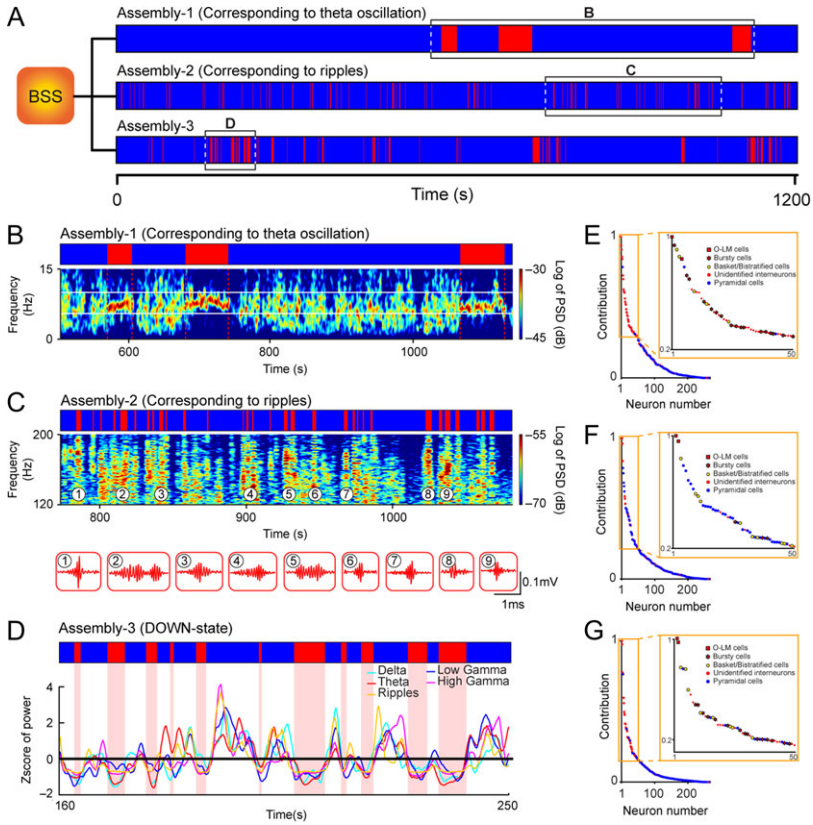

Figure 3. CA1 cell assemblies underlied different sleep cycles. (*A*) Three information source (ISs)-based ensemble patterns are decoded by the iCAD method during the animal's sleep. (*B*) Assembly-1 corresponded to the theta oscillation stage. The upper bar shows the activities of decoded theta ensemble pattern, the red blocks denote the activations of Assembly-1, while the blue blocks represent its inactivity. The power spectrogram below shows the simultaneously recorded local field potential activity within 0–15 Hz frequency band, the theta band (6–10 Hz) is highlighted by white lines. The decoded ensemble pattern is in complete correspondence with the elevated theta band activity (as shown by the red dashed lines). (*C*) Assembly-2 corresponded to ripples. Nine ripple waveforms are replotted below. The ripple-band (120–200 Hz) power spectrogram is shown in the lower subpanel for verifying the accuracy of the cell-assembly decoding result. (*D*) Assembly-3 corresponded to the DOWN-state. Z-scores of power for well-defined frequency bands (Delta, Theta, Low Gamma, High Gamma, and Ripples), where the black line (Z-score = 0) denotes the mean power in each band. It can be observed that the ensemble pattern of Assembly-3 is consistently time-locked with the troughs of these LFP frequency bands. (*E*) Analyses of different cell types which constituted Assembly-1. Most cell members of Assembly-1 were putative interneurons. (*F*) Top tanking cells in Assembly-2 were mostly putative pyramidal cells. (*G*) Cell-type analyses of Assembly-3 show that its members were mostly interneurons.

were mostly putative pyramidal cells (Fig. 3*F*). It is worthwhile to note that many nonmember cells also showed rate changes between ripple epochs versus nonripple periods. Yet, they were distinct from Assembly-2 cells as evidenced by the significant difference in their correlation (Fig. S8*C*).

As for Assembly-3 cells (Fig. 3*D*), we found that they also consisted of mostly interneurons (Fig. 3*G*). But many of them were different from those interneurons listed in Assembly-1 (Fig. S9). It was repeatedly noticed that several cells (~15%) were cross-listed in multiple-sleep oscillatory patterns. The best example is that the same putative O-LM cells were repeatedly identified in all 3 sleep assemblies. Overall, these 3 distinct cell assemblies identified by the self-information coding scheme consistently showed significantly higher correlations among themselves, in comparison to across populations (Fig. S8*D*). The above results demonstrated that the unbiased iCAD method has enabled us to identify distinct cell assemblies that were time-locked to distinct sleep LFP oscillations.

Identification of CA1 Cell Assemblies Underlying Spatial Navigation

To further demonstrate the generality of the self-information coding concept, we asked whether the iCAD method could be used to identify CA1 place cells, which exhibit increased firing indicating place location during navigation (Wilson and McNaughton 1994; Fenton and Muller 1998; Harris et al. 2003; Maurer et al. 2006; Diba and Buzsaki 2007; Pastalkova et al. 2008; Buzsaki 2010; Dupret et al. 2010; Gupta et al. 2010; Kelemen and Fenton 2016; Trimper et al. 2017). We applied the self-information decoding iCAD method to 20-min spike trains of 266 simultaneously recorded CA1 units from a mouse, which was well-trained to run back and forth on a 1 m linear track (without using trial-averaging spike counts over spatial pixels). Based on the minimum CV as the best relevant dimension, our iCAD method unbiasedly revealed 2 distinct CA1 cell-ensemble patterns (Fig. 4*A*). As we aligned these 2 cell-assembly patterns with a videotape that recorded the animal's navigational positions and behaviors on the linear track, we found that these 2 real-time ensemble patterns were nicely matched to the westbound and eastbound navigations, respectively (Fig. 4*B*). Then, we examined top-ranking members from each cell assembly based on their matrix weights and performed position-firing analysis of these cells. A closer examination of the top-weighted CA1 neurons listed in these 2 cell assemblies revealed that some of these cells exhibited classic single place fields (Fig. 4*C*). Many of other cells also showed multiple place fields

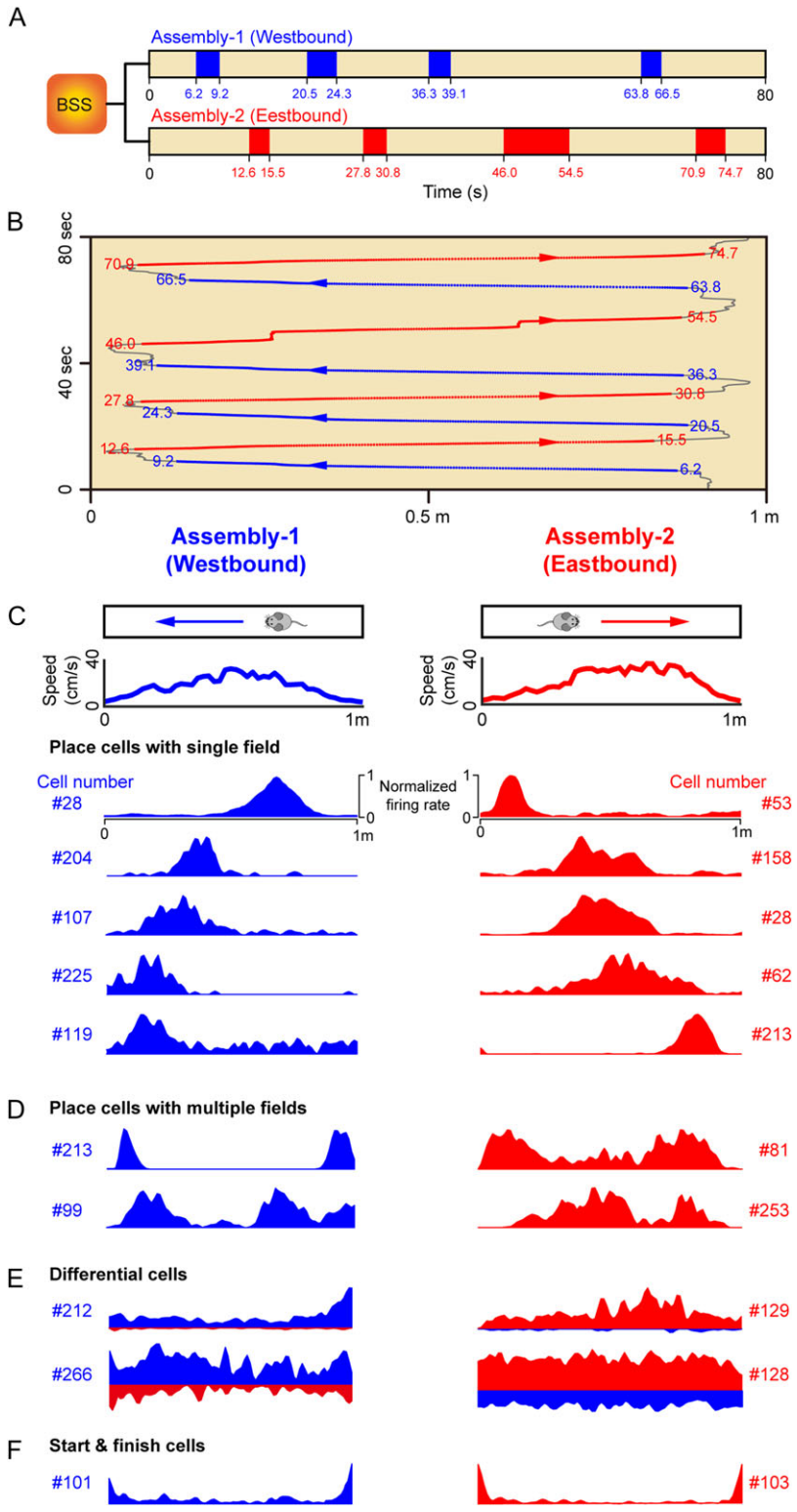

Figure 4. CA1 cell assemblies encoding place fields or start/finish experiences on a linear track. (*A*) Two information source (ISs)-based ensemble patterns were decoded by the iCAD method. The blue/red blocks denote the activations of each corresponding ensemble patterns. (*B*) The animal's trajectory within the 80 s during the linear track experiment (1-m length). Blue dots and arrows denote the decoded ensemble pattern corresponding to "Westbound," while red dots and arrows are for "Eastbound." (*C–F*) Firing patterns of top-weight member cells in 2 cell assemblies. The averaged running speed is shown beneath the linear track illustrations. These top-weight cells fall into 4 categories: Place cells with single place field (*C*), place cells with 2 place fields (*D*), direction-dependent differential firing cells (*E*), ($P < 0.001$ through pairwise *t*-test) and (*F*), start/finish cells that suppressed their firings during navigation. Two start/finish cells is westbound or eastbound specific, respectively.

(Fig. 4D). Among the list, we also noticed that some of the top-contributing CA1 cells did not exhibit discrete place field(s), rather they had differential responses corresponding to directional routing as the mouse traveled westbound or eastbound (Fig. 4E), that is, some CA1 cells preferentially fired in one travel direction over the other.

Unexpectedly, from the list of the iCAD-identified cell assemblies, we also found that both the eastbound and westbound cell assemblies contained cells signaling start/finish transitions; that is, these cells specifically decreased their firing at the start of running and remained low-firing until the end of the navigation (Fig. 4F). While we found 2 start/finish cells engaged in both the westbound and eastbound journals, most interestingly, several CA1 start/finish cells exhibited journal- or direction-specific firing decreases (Fig. 4F, Unit-101 in the left subplot vs. Unit-103 in the right subplot; also see Fig. S10). Such route-specific start/finish responses strongly suggest that the information coded by these cells were not merely corresponding to changes in motion states such as speed acceleration/deceleration, but journey-specific episode(s). Therefore, the neural self-information coding concept has successfully allowed the uncovering of CA1 place cells and their other assembly members, such as start/finish cells, important in accounting for multiple aspects of navigation-related variables.

Prefrontal Cell Assemblies Encoding 5-Choice Visual-Discrimination Behaviors

Finally, we applied the neural self-information concept to uncover novel cell assemblies in the prefrontal cortex related to the 5-choice serial-reaction time (5CSRT), visual-discrimination operant-conditioning behavior—one of the most classical tasks requiring a set of visually and spatially guided attentional procedural actions. In this task, mice learned to nose-poke in 1 of the 5 temporarily lit apertures within a short time window in order to receive a food reward delivered from the food magazine located on the opposite side of the chamber. The mice were trained to reach an 80% success rate (see Materials and Methods). A successful trial typically included the 5-s illumination of 1 of the 5 apertures (in a randomized fashion) to signal the beginning of the trial. During this time, the mouse needs to run from the food magazine area to the response aperture area and then nose-poke in the transiently lit aperture (correct responses), which resulted in a single food pellet being dropped onto the food dish from the magazine. The mouse then runs back to the food magazine area to eat the pellet, which triggers the next trial. A single session typically consisted of 50 trials or more, during which mice performed this attentive choice-action task.

We used 128-channel tetrode arrays and recorded from the PRL while well-trained mice performed this operant-conditioning task. A total of 100 PRL cells were identified as a well-isolated unit and used for the present analysis (those units that did not meet the criterion were excluded). We then scanned the spike dataset consisting of these PRL units using the iCAD method, and a total of 7 cell-assembly patterns were unbiasedly detected. We then aligned the temporal occurrences of these 7 distinct patterns with the recorded videotape and found that all of them could be temporally matched to distinct stages of the operant-procedural task (Fig. 5A, the sequential ensemble patterns from 3 back-to-back trials were plotted).

The PRL assembly-1 pattern was time-locked to the cue-onset when the stimulus aperture was transiently lit for 5 s, signaling the initiation of the 5-choice, visual-discrimination task (Fig. 5A,B). The perievent spike raster and histogram confirmed that Assembly-1 cells exhibited significant changes upon the aperture light on (Fig. 5B, Stage-1). For example, a top-ranking PRL unit increased its firing upon the light on in the stimulus aperture (5-s duration). The firing of this attentive cell then tapered off gradually (Fig. 5B, listed in Start. Upper PTSH subplots). Another PRL cell suppressed its firing upon the stimulus aperture light on [(Fig. 5B) Start. Bottom PTSH subplots].

The PRL assembly-2 activation pattern was time-locked to the first cue-conditioned operant action—namely, running towards the light-lit stimulus aperture from the reward zone toward where the animal was originally located (Fig. 5B, Stage-2; 2 PRL cells are shown). The orientation-firing polar histograms of comparing these cells' activity patterns during the 5-choice, visual-discrimination operant task with those during home-cage running behavior showed that these firings were specific to the operant-conditioning task (Fig. S11A).

The PRL assembly-3 pattern corresponded to the entering of the poke zone (the region near apertures) (Fig. 5B, Stage-3). The place-firing analysis method confirmed that these large-weight responsive PRL units exhibited poke zone-specific spatial firing patterns (2 cells were listed in the upper and lower subpanels, respectively).

Firing patterns of the PRL assembly-4 cells were time-centered around the preparation and the actions of nose-poking at the transiently lit apertures (Fig. 5B, Stage-4). The perievent spike histogram analysis revealed that these units exhibited dynamic firing changes around the nose-poking action. One representative PRL cell exhibited transient suppression during poking of the stimulus aperture (the upper PTSH subpanels), whereas another cell peaked its firing during the preparation phase of nose-poking (lower subpanels), consistent with the role of prefrontal cells in the action planning of goal execution.

The PRL assembly-5 pattern corresponded to the fourth action phase—namely, running back from the poke zone toward the reward zone where the food magazine was located (Fig. 5B, Stage-5). The orientation-firing polar histograms revealed elevated firing changes by these types of member cells. Again, these PRL cells did not show any significant firing changes when the mouse was running around in its home-cage environment (Fig. S11B), suggesting that these cells were goal oriented.

Increased firings of the PRL assembly-6 cells were time-matched to the animal's arrival in the reward zone (Fig. 5B, Stage-6, 2 example cells were listed). These cells' location-specific firing changes were evident from the PTSH plots; again, their spatial positions at the reward zone.

Finally, the Assembly-7 cells decoded by the iCAD method responded to the consumption of food pellets. These PRL cells either increased or decreased their firings (Fig. 5B, Stage-7, 2 cells were shown). While many of the above cells tended to be specific to a given phase of the 5-choice, operant-conditioning task, we noted that some of the cells participated in multiple cell assemblies. For example, some PRL cells belonged to both the running-action assembly and stimulus-aperture zone assembly (Fig. S11C). Other PRL cells would exhibit bidirectional firing during navigation toward the aperture zone (Assembly #2) and reward zone (Assembly #5) (Fig. S11D), or showed goal-approaching-related firing increases in both the poke zone (Assembly #3) and the reward zone (Assembly #6) (Fig. S11E). The above results demonstrated that the self-information coding concept was useful in discovering a variety of prefrontal cell assemblies engaged in distinct stages of the 5-choice, attentive operant-conditioning task.

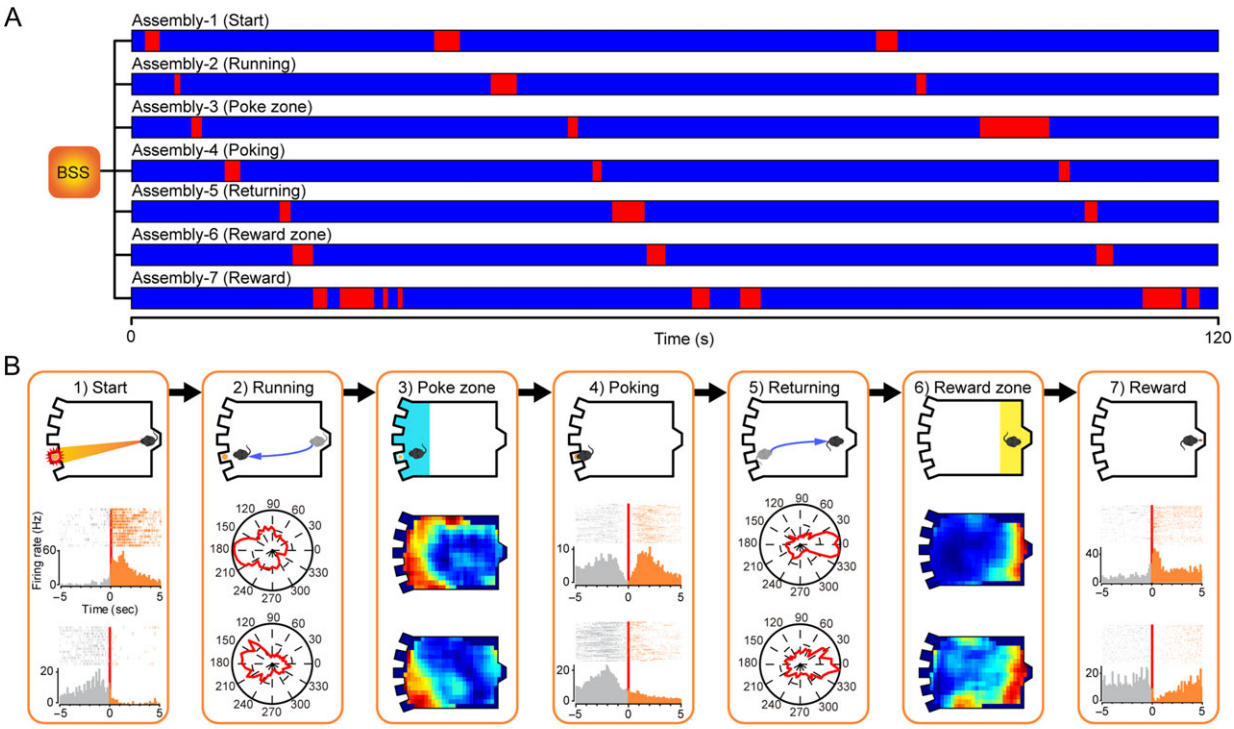

Figure 5. Seven PRL cell assemblies corresponding to each of the 7 stages of 5CSRT behaviors. (*A*) Activations of 7 decoded ensemble patterns during 3 back-to-back trials of 5CSRT visual-discrimination operant-conditioning task. Each ensemble pattern corresponds to 1 of 7 distinct stages of this task. (*B*) Illustrations of 7 decoded ensemble patterns and examples of top large-weight cells in each cell assembly. Stage-1 (Start) Assembly corresponds to the moment which visual stimulus (the illumination of the aperture light on) was presented in 1 of 5 spatial locations to start a trial. Perievent rasters/histograms of 2 example cells exhibited significant increased/decreased firing activities upon the illumination of the aperture light (time = 0). These 2 cells were anticorrelated, the correlation coefficient between these 2 cells was −0.337. Stage-2 (Running) Assembly corresponds to the route when the animal runs from the food magazine region to response-aperture region. Orientation-firing polar histograms of 2 large-weight cells show obvious orientational preferences. Stage-3 (Poke zone) Assembly was activated when the animal was near the response apertures. Apparent spatial-specificity firing patterns of top-contributed cells were observed when the place-cell analysis was applied. Stage-4 (Poking) Assembly corresponds to the poking of the response aperture. Obvious Significant firing changes were observed upon the poking (time = 0) in the perievent rasters/histograms of top-contributed cells. Stage-5 (Returning) Assembly was activated when the animal was running back from the response apertures to the food magazine. Orientational preferences of cell-assembly members were shown. Stage-6 (Reward zone) Assembly corresponds to the locations near the food magazine. Place cell analyses verify that the cell-assembly members exhibited higher firing probabilities within the location near the food magazine, perhaps anticipiating rewards. Stage-7 (Reward) Assembly corresponds to the actions of collecting the reward pellet. Increased/decreased firing activities of 2 cell-assembly members are shown in the perievent rasters/histograms.

Critical Boundaries for ISI-Surprisals to Construct Robust Cell-Assembly Code

The ability to uncover a variety of cell assemblies from multiple brain regions and under multiple conditions and tasks suggest that neural self-information coding represents a general process. The next critical question is whether there is a threshold or boundary in the ISI variability distribution that can efficiently signal the shift from the high-probability ground state into the low-probability surprisal states that would give rise to robust assembly-level neural coding. We approached this question by systematically shifting the positive- and negative-surprisal thresholds from 5% to 45% of the skewed ISI gamma-distribution tails (Fig. 6*A*). We calculated the cell-assembly coherence index by systematically comparing each assembly's temporal dynamics obtained from a given threshold with those obtained from all other thresholds. We found that the sliding of the surprisal thresholds or boundaries between 5% and 15% (ISI variability falling into the low-probability distribution tails) had little effect in terms of improving cell-assembly coherences, whereas assembly-pattern coherence fell apart as the surprisal thresholds shifted from 15% to 30% probability-distribution (Fig. 6*B*). This steep transition around 20% distribution skewed tail was consistently observed in all 15 cell assemblies obtained from different brain regions, mental states and behavioral tasks (Fig. S12). This strongly suggests that there is a conserved and critical boundary transition for constructing efficient self-information neural codes.

Composition of Positive and Negative ISI Surprisals is Region- and Task-Specific

Finally, we explored how dynamic firing changes in putative principal-excitatory cells and interneurons would contribute as positive- or negative-ISI surprisals to construct various cell assemblies (Fig. 7*A*). We first calculated the percentages of positive or negative surprisals out of the total surprisal occurrences in each of the 15 cell-assembly patterns (Fig. 7*B–E*). We then examined how many of these positive or negative surprisals were contributed by the putative excitatory neurons and interneurons. We noted that the majority of cell-assembly members identified in the present study were putative excitatory cells (70.73% in ACC cell assemblies, 78.8% of the total number of CA1 cell assemblies' members, and 80% in PRL cell assemblies), while the rest were fast-spiking interneurons and unclassified neural types (e.g., units with low-firing rates and narrow spike waveforms). As expected, both excitatory neurons and fast-spiking

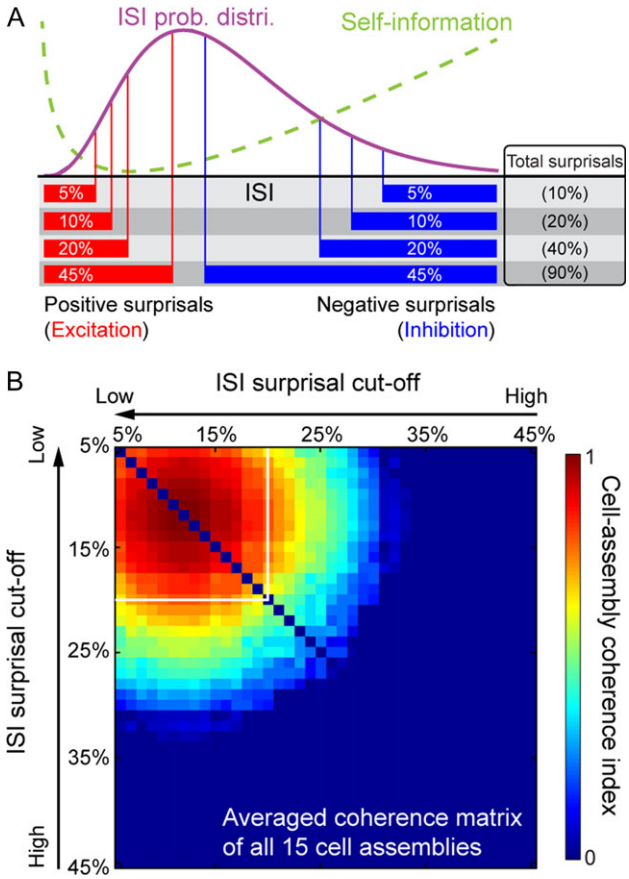

Figure 6. Boundaries for surprisal ISIs in producing robust cell-assembly codes. (*A*) Illustration of applying the sliding-window technique to shift the positive- and negative-surprisal thresholds from 5% (low occurrence probability) to 45% (high occurrence probability) of the skewed ISI gamma-distribution tails. (*B*) The averaged cell-assembly coherence matrix of all 15 cell assemblies in relationship with the ISI surprisal cut-off boundary. Colors in the matrices denote corresponding cell-assembly coherence indexes. Robust cell-assembly patterns were observed with an variability probability of less than 20% of ISIs (as denoted by white square frames in cell-assembly coherence matrices).

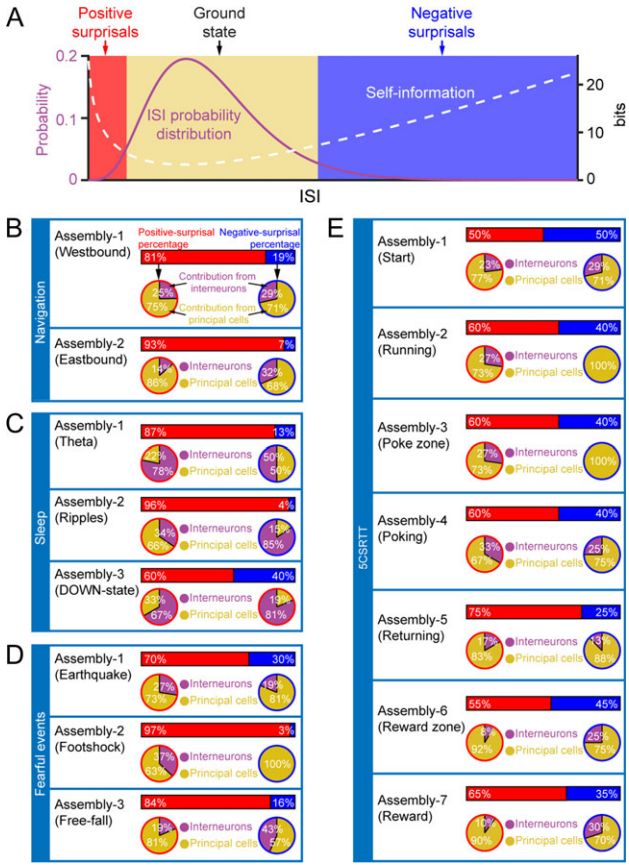

Figure 7. Cell-assembly codes were made of different compositions of positive- and negative-surprisals generated by excitatory neurons and interneurons. (*A*) Cell-assemby patterns emerge as the ternary code: positive surprisals, negative surprisals and the ground state based on cell members' each ISI (in the reverted relationship to neurons' ISI variability probability history). (*B–E*) Percentages of positive surprisals (red bars) or negative surprisals (blue bars) that were used in various cell-assembly codes (*B*. Spatial navigation; *C*. Sleep cycles; *D*. Fearful events; and *E*. 5CSRT). The pie charts showed the percentages of the excitatory neurons (yellow) or interneurons (purple) participated in the form of positive or negative surprisals during each experience or task. 5CSRT task recruited a higher proportion of negative surprisals, reflecting the inhibitory control functions of the PFC in this attention-based behavior.

interneurons can contribute to positive and negative surprisals by increasing or decreasing their ISI time durations. However, we found that the percentages of positive and negative surprisals varied dramatically from one assembly pattern to another, depending on the type(s) of the nature of mental states or tasks. For example, for coding sleep oscillation states—such as theta cycles or ripples, spatial navigation, or processing distinct fearful experiences—these cortical and hippocampal assemblies consisted of overwhelmingly positive surprisals (70–96% of total surprisals) (Fig. 7*B–D*). While excitatory cells contribute overwhelmingly to positive surprisals (due to their large proportion in terms of the total percentage of cell numbers), we noted that fast-spiking interneuron members can be dominant in producing both the positive and negative surprisals in some cases (e.g., CA1 assemblies during sleep).

Most interestingly, various neural coding constructed by PRL cell-assembly patterns (Fig. 7*E*, Assembly-1, 2, 3, 4, 6, and 7) during a 5-choice, visual-discrimination, operant-conditioning task, as well as the CA1 Assembly-3 pattern encoding the downstate of sleep cycle (Fig. 7*C*), were constructed by a large proportion of negative surprisals (40–50% of total surprisals). Therefore, the underlying compositions (i.e., positive and negative surprisals, as well as the percentages of excitatory neurons vs. interneurons) were specific to neural circuits, cognitive states and behavioral tasks.

Discussion

How the brain uses spike patterns to generate real-time neural code is of considerable scientific interest. The key concept of the self-information theory is that, by definition, the amount of self-information contained in a probabilistic event depends only on the probability *P* of that event. Therefore, based on the neuron's ISI-variability probability-distribution, higher-probability ISIs which reflect the balanced excitation-inhibition ground state convey minimal information, whereas lower-probability ISIs which signify rare-occurrence surprisals, in the form of positive or negative surprisals, carry the most information. The self-information-based neural code is interesting to us for the following reasons:

- First, this form of neural code is intrinsic to neurons themselves, with no need for outside observers to set any reference

point followed by artificial bin (i.e., 100 ms per bin)-based pooling methods as used in the rate-code and synchrony-code models. This is because positive or negative ISI surprisals represent significant shifts in biochemical reaction equilibriums, and are instantly coupled to the membrane potentials, energy metabolism, signaling cascades, protein and gene expression levels.

- Second, this self-information code inherently relies on the ISI variability-probability to convey information, whereas neuronal variability is typically viewed as noise that undermines real-time decoding in the classic rate-code or temporal-code models. The ISI variability is a basic phenomenon (Softky and Koch 1993; Stevens and Zador 1998; Shadlen and Movshon 1999; Li and Tsien 2017), and did not grow larger from lower subcortical regions to higher cognition cortices (Li et al. 2018). The importance of spike variability is evident from the fact the diminished variability (i.e., rhythmic firing) underlies anesthesia-induced unconsciousness (Fig. S2) (Fox et al. 2017; Kuang et al. 2010; Li et al. 2018).
- Third, the robustness of this ISI-based surprisal code also comes from its ternary nature of coding (positive or negative surprisals, plus the ground state). It is noteworthy that negative surprisals use the entire time-duration of the prolonged ISI (silence duration) to carry significant information, whereas the classic temporal code typically focuses on binning spikes across cell population to search for synchrony.
- Fourth, the iCAD method may be useful to explore new ways for the detection of population patterns for the brain-machine interface (Ifft et al. 2013). It will be interesting to examine how transient rhythmic firing, as observed in some interneurons during motor task-initiation period (Lebedev and Nelson 1995), contributes to and/or regulates self-information patterns in their target cells. One may further explore higher-level (second-order) self-information beyond a single ISI by analyzing serial timing information between multiple adjoining spikes (Perkel et al. 1967).

Overall, we have successfully applied the self-information concept and uncovered 15 cell assemblies from the PRL, ACC, and hippocampal CA1. In the ACC, we identified 3 cell-assembly patterns corresponding to categorical variables such as earthquake, elevator-drop or mild electric footshock experiences, consistent with its crucial role in processing emotions and fear behaviors (Kim and Jung 2006; Steenland et al. 2012; Xie et al. 2013; Giustino et al. 2016; Zhuo 2016). We noted that many ACC cells exhibited specific responses to a specific fearful experience (i.e., earthquake vs. footshock), whereas some cells responded in a combinatorial manner, such as coding for both earthquake and footshock, or earthquake and free-fall, etc. Moreover, some ACC cells participated in all cell assemblies, reflected by their responsiveness to all 3 fearful events. Such specific-to-general combinatorial cell assemblies in the ACC is highly consistent with the recent finding that the brain computation is organized by the power-of-two permutation-based logic (Tsien 2015; Xie et al. 2016). We further assessed the stability of ACC cell assembly by comparing the top cells (based on the weight matrix using first and second halves trials). We found that ~75% of fear-memory coding cell-assembly members remained stable in the ACC.

In the hippocampal CA1, we found not only classic place cells with a single salient place field (Wilson and McNaughton 1994; Fenton and Muller 1998; Csicsvari et al. 1999; Harris et al. 2003; Maurer et al. 2006; Buzsaki 2010; Dupret et al. 2010; Trimper et al. 2017), but also cells with multiple place fields (Fenton et al. 2008; Park et al. 2011) or differential firing cells between the eastbound versus westbound. These cells with irregular multiple-place fields often occupied the top-ranking memberships in the demixing matrix $\mathbf{W}$. Moreover, we have discovered some CA1 cells responding to the start and finish state. Because many of these "start/finish cells" were specific to either the westbound or eastbound journey, this suggests that their firing changes were not simply reflecting generic motion transition. These start/finish cells may encode the episodic concept of the start and finish for marking a unique journey.

We also found the existence of 3 CA1 assembly patterns that were time-locked with theta, ripples, and downstate cycles during sleep. To our knowledge, it is the first unbiased method to allow researchers to define cell-assembly memberships underlying sleep. Traditional classification, based on spike-phase coupling (theta coupled cells vs. noncoupled cells), would have predicted that all sleep theta-coupled cells would belong to the same assembly. Similarly, the same prediction would also apply to ripple-coupled cells versus nonripple-coupled cells. While many theta-coupled or ripple-coupled CA1 cells were extensively studied during sleep (Fox et al. 1986; Wilson and McNaughton 1994; Csicsvari et al. 1999; Cantero et al. 2003; Somogyi and Klausberger 2005; Diba and Buzsaki 2007; Eschenko et al. 2008; Klausberger and Somogyi 2008; Pastalkova et al. 2008; Kuang et al. 2010; Colgin 2016; Sara 2017), surprisingly, we found that many of them did not belong to this sleep theta cell assembly or the ripple cell assembly. Their distinct memberships were further supported by their distinct correlations (Fig. S8). This finding will open a door to analyze further how distinct cell populations engage sleep-related functions.

In the PRL, we uncovered 7 distinct real-time cell assemblies that were time-locked to the onset of cues and cue-induced behavioral actions. Their sequential activation matched nicely to each stage of 5-choice, visual-discrimination, operant-conditioning actions. Within the first cell assembly, there are multiple subtypes of cells that exhibited different time courses of responses. One type reacted to ramping activity prior to the onset of the cue (light on in the stimulus aperture) (Fig. 5*B*, the bottom PTSH subpanel), perhaps reflecting preparatory (pre-cue) attention in such attentional tasks (Totah et al. 2009; Kim et al. 2016). One noticeable feature in the PRL assembly codes is the apparent recruitment of large proportions of negative surprisals for encoding both categorical-variable patterns ("start," "poking," and "reward") and continuous-variable patterns ("running," "poke zone," "returning," and "reward zone") (Fig. 7*E*). This supports the notion that the PRL exerts its strong inhibitory control to the downstream targets via using negative ISI surprisals during the attentional tasks.

Finally, we investigated whether there is a critical boundary in defining ISIs representing the ground state versus the positive and/or negative surprisals. Our analyses revealed a steep transition in deploying ISI surprisals, around 20% of the skewed ISI gamma-distribution tails, to generate efficient real-time cell-assembly codes. The majority (80%) of remaining ISIs operated as the ongoing low-information ground states. This 80/20 statistical rule is surprisingly consistent with the Pareto Principle of factor sparsity (Hardy 2010), which states that, for many events (i.e., in communication or resource management), roughly 80% of the output or consequences stem from 20% of the input or causes (Juran et al. 1950; Ultsch 2002; Hardy 2010). While the ground state corresponds to the most probable ISIs which carry less self-information, it should not be viewed as wasting energy. The ground state ISIs constitute the online state that not only enables the rapid responses to changes, but also the

construction of ternary codes (together with the positive and negative surprisals), leading to the enormous coding capacity far superior to the binary coding of current computers (Li and Tsien 2017). Imposing this ternary coding onto the cell assemblies organized by the power-of-two-based permutation logic, together they form the cornerstone for the basic brain computation, giving rise to real-time cognitions and intelligent behaviors (Tsien 2015; Xie et al. 2016).

In summary, in contrast to the traditional view that enormous spike variability reflects noise, we tested the Neural Self-Information theory that the ISI, or the silence duration between 2 adjoining spikes, carries self-information that solely depends on its inverted relation to its probability against the neuron's ISI variability history. We applied this novel concept and showed that neural code uses ISI variability as the real-time self-information messenger to encode cell-assembly patterns. Analysis of 15 uncovered cell assemblies suggests the existence of conserved critical boundaries in utilizing ~20% of ISIs as surprisals to generate real-time representations of cognition and behavior. Spike-variability-based neural coding principle can also provide new interpretations for many optogenetic experiments in which a fixed stimulation-frequency was repeatedly delivered to a given cell type.

Supplementary Material

Supplementary material is available at *Cerebral Cortex* online.

Author Contributions

J.Z.T. and M.L. conceived and designed the project. J.Z.T. designed the experiments with M.L., K.X., H.K., G.E.F., and J.L. The research was performed as follows: K.X. recorded from the ACC and PRL datasets; G.E.F. from the RSC; Jun Liu from the BLA; D.W. from the striatum, H.K. from the CA1. M.L., F.Z., H.K., Z.S., L.C., and Y.M. for data analyses together with J.Z.T. J.Z.T. and M.L. wrote the article with input from all others.

Funding

NIH grant (R01NS079774), US Army grant (W911NF-17-1-0534), NSF ABI Innovation grant (1564736) and GRA *Brain Decoding Project* to J.Z.T., Shanghai Youth Science and Technology Sail Project (16YF1415200) to Z.S., M.L. and the Brain Decoding Center grant from the Department of Science and Technology of Yunnan Province (2014DG002) to F.Z. and J.Z.T.

Notes

We thank Fengying Huang for maintaining the mouse colony and training the mice for the 5-choice, operant-conditioning tasks, and Sandra E. Jackson for proofreading this article. *Conflict of Interest*: None declared.

References

Abbott LF, Dayan P. 1999. The effect of correlated variability on the accuracy of a population code. Neural Comput. 11(1):91–101.

Abbott L, Sejnowski TJ. 1999. Neural codes and distributed representations: foundations of neural computation. Cambridge, MA: Mit Press.

Adrian ED, Zotterman Y. 1926. The impulses produced by sensory nerve endings: Part 3. Impulses set up by Touch and Pressure. J Physiol. 61(4):465–483.

Arieli A, Sterkin A, Grinvald A, Aertsen A. 1996. Dynamics of ongoing activity: explanation of the large variability in evoked cortical responses. Science. 273(5283):1868–1871.

Averbeck BB, Latham PE, Pouget A. 2006. Neural correlations, population coding and computation. Nat Rev Neurosci. 7(5):358–366.

Bliss TVP, Collingridge GL, Kaang B-K, Zhuo M. 2016. Synaptic plasticity in the anterior cingulate cortex in acute and chronic pain. Nat Rev Neurosci. 17(8):485–496.

Buzsaki G. 2010. Neural syntax: cell assemblies, synapsembles, and readers. Neuron. 68(3):362–385.

Buzsaki G, Buhl DL, Harris KD, Csicsvari J, Czeh B, Morozov A. 2003. Hippocampal network patterns of activity in the mouse. Neuroscience. 116(1):201–211.

Cantero JL, Atienza M, Stickgold R, Kahana MJ, Madsen JR, Kocsis B. 2003. Sleep-dependent theta oscillations in the human hippocampus and neocortex. J Neurosci. 23(34):10897–10903.

Churchland MM, Yu BM, Cunningham JP, Sugrue LP, Cohen MR, Corrado GS, Newsome WT, Clark AM, Hosseini P, Scott BB, et al. 2010. Stimulus onset quenches neural variability: a widespread cortical phenomenon. Nat Neurosci. 13(3):369–378.

Colgin LL. 2016. Rhythms of the hippocampal network. Nat Rev Neurosci. 17(4):239–249.

Csicsvari J, Hirase H, Czurko A, Mamiya A, Buzsaki G. 1999. Oscillatory coupling of hippocampal pyramidal cells and interneurons in the behaving Rat. J Neurosci. 19(1):274–287.

Diba K, Buzsaki G. 2007. Forward and reverse hippocampal place-cell sequences during ripples. Nat Neurosci. 10(10):1241–1242.

Dupret D, O'Neill J, Pleydell-Bouverie B, Csicsvari J. 2010. The reorganization and reactivation of hippocampal maps predict spatial memory performance. Nat Neurosci. 13(8):995–1002.

Eschenko O, Ramadan W, Molle M, Born J, Sara SJ. 2008. Sustained increase in hippocampal sharp-wave ripple activity during slow-wave sleep after learning. Learn Mem. 15(4):222–228.

Faisal AA, Selen LP, Wolpert DM. 2008. Noise in the nervous system. Nat Rev Neurosci. 9(4):292–303.

Fenton AA, Kao H-Y, Neymotin SA, Olypher A, Vayntrub Y, Lytton WW, Ludvig N. 2008. Unmasking the CA1 ensemble place code by exposures to small and large environments: more place cells and multiple, irregularly arranged, and expanded place fields in the larger space. J Neurosci. 28(44):11250–11262.

Fenton AA, Muller RU. 1998. Place cell discharge is extremely variable during individual passes of the rat through the firing field. Proc Natl Acad Sci USA. 95(6):3182–3187.

Fox GE, Li M, Zhao F, Tsien JZ. 2017. Distinct retrosplenial cortex cell populations and their spike dynamics during ketamine-induced unconscious state. PLoS One. 12(10):e0187198.

Fox SE, Wolfson S, Ranck JB Jr. 1986. Hippocampal theta rhythm and the firing of neurons in walking and urethane anesthetized rats. Exp Brain Res. 62(3):495–508.

Giustino TF, Fitzgerald PJ, Maren S. 2016. Fear expression suppresses medial prefrontal cortical firing in rats. PLoS One. 11(10):e0165256.

Gupta AS, van der Meer MA, Touretzky DS, Redish AD. 2010. Hippocampal replay is not a simple function of experience. Neuron. 65(5):695–705.

Hardy M. 2010. Pareto's law. Math Intell. 32(3):38–43.

Harris KD, Csicsvari J, Hirase H, Dragoi G, Buzsaki G. 2003. Organization of cell assemblies in the hippocampus. Nature. 424(6948):552–556.

Hartmann C, Lazar A, Nessler B, Triesch J. 2015. Where's the noise? Key features of spontaneous activity and neural variability

arise through learning in a deterministic network. PLoS Comp Biol. 11(12):e1004640.
Ifft PJ, Shokur S, Li Z, Lebedev MA, Nicolelis MA. 2013. A brain-machine interface enables bimanual arm movements in monkeys. Sci Transl Med. 5(210):210ra154.
Juran J, Pareto L, Carnot B. 1950. Juran and others. Ind Qual Control. p. 25.
Kanitscheider I, Coen-Cagli R, Pouget A. 2015. Origin of information-limiting noise correlations. Proc Natl Acad Sci USA. 112(50):E6973–E6982.
Kelemen E, Fenton AA. 2016. Coordinating different representations in the hippocampus. Neurobiol Learn Mem. 129: 50–59.
Kim H, Ahrlund-Richter S, Wang X, Deisseroth K, Carlen M. 2016. Prefrontal parvalbumin neurons in control of attention. Cell. 164(1–2):208–218.
Kim JJ, Jung MW. 2006. Neural circuits and mechanisms involved in Pavlovian fear conditioning: a critical review. Neurosci Biobehav Rev. 30(2):188–202.
Klausberger T, Somogyi P. 2008. Neuronal diversity and temporal dynamics: the unity of hippocampal circuit operations. Science. 321(5885):53–57.
Kohn A, Coen-Cagli R, Kanitscheider I, Pouget A. 2016. Correlations and neuronal population information. Annu Rev Neurosci. 39:237–256.
Kuang H, Lin L, Tsien JZ. 2010. Temporal dynamics of distinct CA1 cell populations during unconscious state induced by ketamine. PLoS One. 5(12):e15209.
Lebedev MA, Nelson RJ. 1995. Rhythmically firing (20–50 Hz) neurons in monkey primary somatosensory cortex: activity patterns during initiation of vibratory-cued hand movements. J Comput Neurosci. 2(4):313–334.
Lee D, Port NL, Kruse W, Georgopoulos AP. 1998. Variability and correlated noise in the discharge of neurons in motor and parietal areas of the primate cortex. J Neurosci. 18(3):1161–1170.
Li M, Liu J, Tsien JZ. 2016. Theory of Connectivity: Nature and Nurture of Cell Assemblies and Cognitive Computation. Front Neural Circuits. 10:34.
Li M, Tsien JZ. 2017. Neural code—neural self-information theory on how cell-assembly code rises from spike time and neuronal variability. Front Cell Neurosci. 11:236.
Li M, Xie K, Kuang H, Liu J, Wang D, Fox GE, Wei W, Li X, Li Y, Zhao F. 2018. Spike-timing pattern operates as gamma-distribution across cell types, regions and animal species and is essential for naturally-occurring cognitive states. Biorxiv. p. 145813.
Lin L, Chen G, Xie K, Zaia KA, Zhang S, Tsien JZ. 2006a. Large-scale neural ensemble recording in the brains of freely behaving mice. J Neurosci Methods. 155(1):28–38.
Lin IC, Okun M, Carandini M, Harris KD. 2015. The nature of shared cortical variability. Neuron. 87(3):644–656.
Lin L, Osan R, Tsien JZ. 2006b. Organizing principles of real-time memory encoding: neural clique assemblies and universal neural codes. Trends Neurosci. 29(1):48–57.
Liu J, Wei W, Kuang H, Tsien JZ, Zhao F. 2014. Heart rate and heart rate variability assessment identifies individual differences in fear response magnitudes to earthquake, free fall, and air puff in mice. PLoS One. 9(3):e93270.
Liu J, Wei W, Kuang H, Zhao F, Tsien JZ. 2013. Changes in heart rate variability are associated with expression of short-term and long-term contextual and cued fear memories. PLoS One. 8(5):e63590.
Luczak A, Bartho P, Harris KD. 2013. Gating of sensory input by spontaneous cortical activity. J Neurosci. 33(4):1684–1695.
Maimon G, Assad JA. 2009. Beyond Poisson: increased spike-time regularity across primate parietal cortex. Neuron. 62(3): 426–440.
Mainen ZF, Sejnowski TJ. 1995. Reliability of spike timing in neocortical neurons. Science. 268(5216):1503–1506.
Marcos E, Pani P, Brunamonti E, Deco G, Ferraina S, Verschure P. 2013. Neural variability in premotor cortex is modulated by trial history and predicts behavioral performance. Neuron. 78(2):249–255.
Maurer AP, Cowen SL, Burke SN, Barnes CA, McNaughton BL. 2006. Organization of hippocampal cell assemblies based on theta phase precession. Hippocampus. 16(9):785–794.
Park E, Dvorak D, Fenton AA. 2011. Ensemble place codes in hippocampus: CA1, CA3, and dentate gyrus place cells have multiple place fields in large environments. PLoS One. 6(7): e22349.
Pastalkova E, Itskov V, Amarasingham A, Buzsaki G. 2008. Internally generated cell assembly sequences in the rat hippocampus. Science. 321(5894):1322–1327.
Perkel DH, Gerstein GL, Moore GP. 1967. Neuronal spike trains and stochastic point processes. I. The single spike train. Biophys J. 7(4):391–418.
Petersen CCH, Hahn TTG, Mehta M, Grinvald A, Sakmann B. 2003. Interaction of sensory responses with spontaneous depolarization in layer 2/3 barrel cortex. Proc Natl Acad Sci USA. 100(23):13638–13643.
Rolls E, Deco G. 2010. The noisy brain. Stochastic dynamics as a principle of brain function (Oxford Univ. Press, UK, 2010).
Saberi-Moghadam S, Ferrari-Toniolo S, Ferraina S, Caminiti R, Battaglia-Mayer A. 2016. Modulation of neural variability in premotor, motor, and posterior parietal cortex during change of motor intention. J Neurosci. 36(16):4614–4623.
Sara SJ. 2017. Sleep to remember. J Neurosci. 37(3):457–463.
Schmitzer-Torbert N, Jackson J, Henze D, Harris K, Redish AD. 2005. Quantitative measures of cluster quality for use in extracellular recordings. Neuroscience. 131(1):1–11.
Scholvinck ML, Saleem AB, Benucci A, Harris KD, Carandini M. 2015. Cortical state determines global variability and correlations in visual cortex. J Neurosci. 35(1):170–178.
Shadlen MN, Movshon JA. 1999. Synchrony unbound: a critical evaluation of the temporal binding hypothesis. Neuron. 24 (1):67–77. 11125.
Shadlen MN, Newsome WT. 1994. Noise, neural codes and cortical organization. Curr Opin Neurobiol. 4(4):569–579.
Softky WR, Koch C. 1993. The highly irregular firing of cortical cells is inconsistent with temporal integration of random EPSPs. J Neurosci. 13(1):334–350.
Somogyi P, Klausberger T. 2005. Defined types of cortical interneurone structure space and spike timing in the hippocampus. J Physiol. 562(Pt 1):9–26.
Steenland HW, Li X-Y, Zhuo M. 2012. Predicting aversive events and terminating fear in the mouse anterior cingulate cortex during trace fear conditioning. J Neurosci. 32(3): 1082–1095.
Stein RB, Gossen ER, Jones KE. 2005. Neuronal variability: noise or part of the signal? Nat Rev Neurosci. 6(5):389–397.
Stevens CF, Zador AM. 1998. Input synchrony and the irregular firing of cortical neurons. Nat Neurosci. 1(3):210–217.
Totah NK, Kim YB, Homayoun H, Moghaddam B. 2009. Anterior cingulate neurons represent errors and preparatory attention within the same behavioral sequence. J Neurosci. 29 (20):6418–6426.

Trimper JB, Trettel SG, Hwaun E, Colgin LL. 2017. Methodological caveats in the detection of coordinated replay between place cells and grid cells. Front Syst Neurosci. 11:57.

Tsien JZ. 2015. A postulate on the brain's basic wiring logic. Trends Neurosci. 38(11):669–671.

Ultsch A. 2002. Proof of Pareto's 80/20 law and precise limits for ABC-analysis. Lahn, Germany: Data Bionics Research Group University of Marburg. p. 1–11.

Wehr M, Zador AM. 2003. Balanced inhibition underlies tuning and sharpens spike timing in auditory cortex. Nature. 426 (6965):442–446.

Wilson MA, McNaughton BL. 1994. Reactivation of hippocampal ensemble memories during sleep. Science. 265(5172):676–679.

Xie K, Fox GE, Liu J, Lyu C, Lee JC, Kuang H, Jacobs S, Li M, Liu T, Song S, et al. 2016. Brain computation is organized via power-of-two-based permutation logic. Front Syst Neurosci. 10:95.

Xie K, Kuang H, Tsien JZ. 2013. Mild blast events alter anxiety, memory, and neural activity patterns in the anterior cingulate cortex. PLoS One. 8(5):e64907.

Zhuo M. 2016. Neural mechanisms underlying anxiety-chronic pain interactions. Trends Neurosci. 39(3):136–145.